JPE 19-5-24

https://doi.org/10.6113/JPE.2019.19.5.1315
ISSN(Print): 1598-2092 / ISSN(Online): 2093-4718

Power Quality Optimal Control of Railway Static Power Conditioners Based on Electric Railway Power Supply Systems

Youhua Jiang*, Wenji Wang†, Xiangwei Jiang**, Le Zhao***, and Yilong Cao*

†State Grid Wuhan Electric Power Company, Wuhan, China
*College of Electronics and Information Engineering, Shanghai University of Electric Power, Shanghai, China
**State Grid Anqing Power Supply Company, Anqing, China
***Shanghai Electric Power Research Institute, Shanghai, China

Abstract

Aiming at the negative sequence and harmonic problems in the operation of railway static power conditioners, an optimization compensation strategy for negative sequence and harmonics is studied in this paper. First, the hybrid RPC topology and compensation principle are analyzed to obtain different compensation zone states and current capacities. Second, in order to optimize the RPC capacity configuration, the minimum RPC compensation capacity is calculated according to constraint conditions, and the optimal compensation coefficient and compensation angle are obtained. In addition, the voltage unbalance ε_U and power factor requirements are satisfied. A PSO (Particle Swarm Optimization) algorithm is used to calculate the three indexes for minimum compensating energy. The proposed method can precisely calculate the optimal compensation capacity in real time. Finally, MATLAB simulations and an experimental platform verify the effectiveness and economics of the proposed algorithm.

Key words: Negative sequence and harmonic, Railway static power conditioner, The minimum RPC compensation capacity

I. INTRODUCTION

High-speed railway networks play an important role in civilian and military fields. Due to the high demands of speed and capacity, the load is gradually rising, and its influence on the power quality of the upper power supply system is becoming increasingly obvious. The railway static power conditioner (RPC) proposed by Japanese scholars can effectively overcome the shortcomings of traditional control devices for the compensation of poor negative sequences and harmonics. In addition, they provide new ideas for controlling the power quality of high-speed railways.

For the topological structure, compensation principle and detection method of an RPC, relevant literature has been elaborated. Since its introduction in 1993, it has only been put into practical application at a few traction substations at home and abroad. In view of this, related literature proposed a hybrid electrified railway power quality comprehensive management system (RPC+SVC hybrid structure) that is suitable for China's national conditions and has a high cost performance. This system has been used for complete compensation or optimization compensation, and it provides for the commercial application of an RPC. RPC compensation is more advantageous than either TCR or TSC compensation. The latter takes up a lot of space, is not conducive to installation, and easily resonates with the grid. The RPC compensation system has flexible control, small occupancy and obvious advantages. However, its larger compensation capacity makes it less practical, which limits the large-scale

Manuscript received Oct. 6, 2018; accepted May 29, 2019
Recommended for publication by Associate Editor Kai Sun.
†Corresponding Author: shuaiwwj@126.com
Tel: +86-18717975317, State Grid Wuhan Electric Power Company
*College of Electronics and Information Engineering, Shanghai University of Electric Power, China
**State Grid Anqing Power Supply Company, China
***Shanghai Electric Power Research Institute, China

utilization of RPC. Thus, it is necessary to optimize the capacity of RPC compensation.

In 2009, RPC was tested at Shanghai Nanxiang, and the test results showed that the RPC compensation effect was good. With the rapid increase of railway loads, the capacity requirements of RPCs are getting larger and larger, and the cost becomes higher. Therefore, if the power factor and unbalance requirements can be met, a minimum negative sequence current compensation method is meaningful.

A lot of research has been carried out on RPCs. The most important problem of RPCs is to decrease negative sequence components [7]. A method based on sequential quadratic programming (SQP) was proposed [2]. The optimization process can be completed in a few milliseconds with the efficiency and accuracy necessary to meet RPC compensation requirements. A hybrid power quality compensation device for managing negative sequence harmonics is also practical. RPCs are mainly used to transmit active power, while reactive power is controlled by thyristor reactors and two thyristors are controlled by filter compensation [3], [4]. In this hybrid compensation system, reactive power is compensated by a SVC, and a RPC is used for active transmission and harmonic suppression. These methods reduce the capacity of the RPC. However, they cannot keep it to a minimum. In order to make the power factor satisfy its requirements, a power factor-oriented RPC compensation strategy can be used [5]. This method has a high controllability and helps to reduce the RPC capacity and improve the control flexibility.

In this paper, a mathematical model under the constraint conditions of compensation capacity, power factor and voltage unbalance limit is established. In order to obtain the optimal compensation coefficient λ and the angle φ, the RPC capacity is optimized. Full compensation means the harmonics and the negative sequence current are eliminated as much as possible. Optimization compensation means that the harmonics and the negative sequence currents are reduced to meet national standard requirements for compensation. This reduces the energy required by the device to compensate. This paper proposes two compensation indicators. These indicators are the compensation coefficient λ and the compensation angle φ. Power analysis is calculated using a Particle Swarm Optimization (PSO) algorithm [29]. Analysis shows that the algorithm can reduce the compensation capacity and improve the electrical energy while meeting the power quality index on a global scope.

Simulation and experimental results verify the validity of the theory. The rest of this paper is organized as follows. The compensation structure and principle analysis are presented in Section II. In Section III, a control strategy of an RPC is proposed, and an optimal compensation based on a PSO algorithm is introduced. Section IV give a number of simulation and experimental results. Finally, the conclusion is provided in Section V.

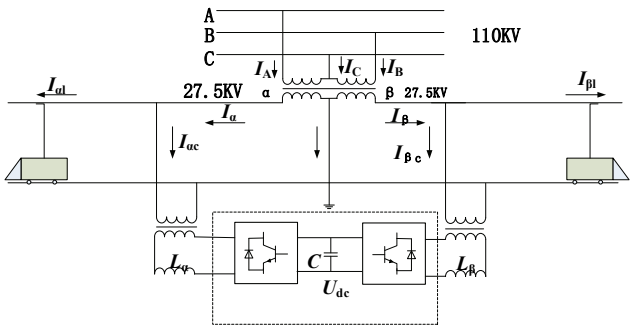

Fig. 1. Topology of an RPC compensation system.

II. Compensation Structure and Principle Analysis of a V/v Traction Power Supply System

An RPC compensation structure is shown in Fig. 1. The electric locomotive is provided with 27.5 kV of single-phase power supply from the left and right two-phase power supply arms, and the three-phase 220 kV bus line supplies power to the two power supply arms via the V/v transformer. The RPC consists of two converters with a common DC capacitor. The high-capacity DC capacitors in parallel between the two converters ensure stable operation. They are connected to the traction power supply arm through a step-down transformer and controlled by the IGBT bridge controlling the converter. The electric energy of the two arms flows to realize the electric energy management of the two power supply arms.

The primary side of the three-phase voltage in the traction transformer is u_A, u_B, u_C. In addition, u_α and u_β are the arm voltages of the secondary side α and β power supplies. i_α and i_β are the α and β power supply arm currents, $i_{\alpha p}$ and $i_{\beta p}$ are the power supply arm active current, and $i_{\alpha q}$ and $i_{\beta q}$ are the power supply arms reactive current.

The V/v traction transformer is composed of two single-phase transformers and installed in an oil tank. The capacity can be designed according to requirements. Thus, both electric phase separation and voltage regulation can be realized. In actual engineering installations, the primary side three-phase terminals are connected with three-phase grid busbars, the secondary side c phase is connected with the rails and the ground, and the secondary sides a and b phases are connected to the contact nets and the corresponding traction power arm, respectively. Let $i_{\alpha L}$ and $i_{\beta L}$ be the load currents of the α phase and the β phase power supply arms, and i_A, i_B, i_C be the primary current of the V/v traction transformer. Let $\gamma=e^{j120^\circ}$ and $i_C = -(i_A + i_B)$. In addition, K represents the transformer ratio. The current relationship between the secondary side of the V/v traction transformer is:

$$\begin{bmatrix} i_A \\ i_B \\ i_C \end{bmatrix} = \frac{1}{K}\begin{bmatrix} 1 & 0 \\ 0 & 1 \\ -1 & -1 \end{bmatrix}\begin{bmatrix} i\alpha \\ i\beta \end{bmatrix} \quad (1)$$

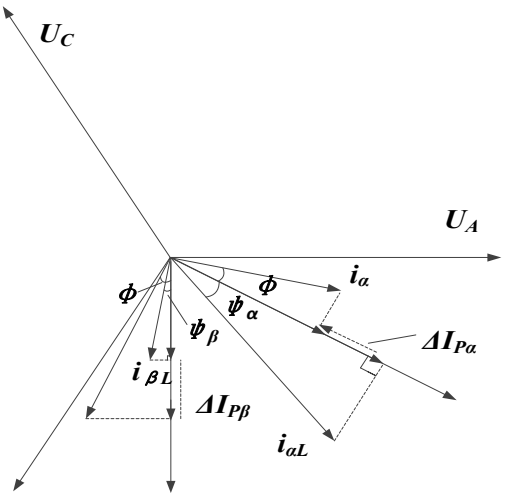

Fig. 2. Current phase diagram of active and reactive power.

Using the symmetrical component method, the three-phase currents i_A, i_B, i_C are decomposed to:

$$\begin{bmatrix} i_1 \\ i_2 \\ i_0 \end{bmatrix} = \begin{bmatrix} 1 & \gamma & \gamma^2 \\ 1 & \gamma^2 & \gamma \\ 1 & 1 & 1 \end{bmatrix} \begin{bmatrix} i_A \\ i_B \\ i_C \end{bmatrix} \tag{2}$$

Inputting (1) into (2) yields (3):

$$\begin{bmatrix} i_1 \\ i_2 \\ i_0 \end{bmatrix} = \frac{1}{K} \begin{bmatrix} i_\alpha + \gamma i_\beta - \gamma^2 (i_\alpha + i_\beta) \\ i_\alpha + \gamma^2 i_\beta - \gamma (i_\alpha + i_\beta) \\ 0 \end{bmatrix} \tag{3}$$

After optimization compensation of the three-phase current, a phasor diagram is shown in Fig. 2. Let the phase difference between the voltages of the two power supply arms and the current after optimization compensation be φ. The active and reactive powers needed for compensation are ΔP_α, ΔP_β and ΔQ_α, ΔQ_β respectively:

$$\begin{cases} \Delta P_\alpha = 0.5\lambda (P_{\beta 0} - P_{\alpha 0}) \\ \Delta P_\beta = 0.5\lambda (P_{\alpha 0} - P_{\beta 0}) \end{cases} \tag{4}$$

$$\begin{cases} \Delta Q_\alpha = Q_\alpha + (P_{\alpha 0} + \Delta P_\alpha) \tan\varphi \\ \Delta Q_\beta = Q_\beta - (P_{\beta 0} + \Delta P_\beta) \tan\varphi \end{cases} \tag{5}$$

Active transfer current is:

$$\Delta I_p = \frac{1}{2} \lambda (I_{\alpha p} - I_{\beta p}) \tag{6}$$

The larger λ is, the more active power is transferred. When λ=1, the RPC performs full compensation of the active power. After compensation, the amplitudes of the active current are:

$$\begin{cases} I'_{\alpha p} = I_{\alpha p} - \frac{I_{\alpha p} - I_{\beta p}}{2} \lambda \\ I'_{\beta p} = I_{\beta p} + \frac{I_{\alpha p} - I_{\beta p}}{2} \lambda \end{cases} \tag{7}$$

After the compensation, the left and right arm currents are:

$$\begin{cases} I'_\alpha = (I_{\alpha p} - \frac{I_{\alpha p} - I_{\beta p}}{2} \lambda) / cos\varphi \\ I'_\beta = (I_{\beta p} + \frac{I_{\alpha p} - I_{\beta p}}{2} \lambda) / cos\varphi \end{cases} \tag{8}$$

The current directions of the two arms α and β are $e^{j(30°-\varphi)}$ and $e^{j(90°+\varphi)}$, respectively. The energy consumed by arm α is:

$$\begin{aligned} S_\alpha &= \sqrt{\Delta P_\alpha{}^2 + \Delta Q_\alpha{}^2} \\ &= U_\alpha \sqrt{\Delta I_p{}^2 + [I_{\alpha q} + (I_{\alpha p} - \Delta I_p) tan\varphi]^2} \end{aligned} \tag{9}$$

Meanwhile, for arm β it is:

$$\begin{aligned} S_\beta &= \sqrt{\Delta P_\beta{}^2 + \Delta Q_\beta{}^2} \\ &= U_\beta \sqrt{\Delta I_p{}^2 + [I_{\beta q} + (I_{\beta p} - \Delta I_p) tan\varphi]^2} \end{aligned} \tag{10}$$

The RPC compensation capacity is also related to the negative sequence imbalance ε_U, and the negative sequence imbalance ε_U satisfies:

$$\varepsilon_U = \varepsilon_1 S_L / S_d \tag{11}$$

According to IEEE Std 1159-1995, the voltage unbalance limit is 2% [18]. Formula (12) can be obtained from the above analysis, and it should satisfy:

$$\begin{cases} min\ (S_\alpha + S_\beta) \\ \varepsilon_U \le 2\% \\ \frac{P_{sum}}{\sqrt{P_{sum}{}^2 + Q_{sum}{}^2}} \in [0.95, 1] \end{cases} \tag{12}$$

$min\ (S_\alpha + S_\beta)$ refers to the energy consumed by the α and β power supply arms, which is required to minimize the energy consumed by the RPC. $\varepsilon_U \le 2\%$ refer to the voltage imbalance constraints. The third equation refers to the power factor constraints. P_{sum} refers to the sum of the primary side three-phase active power, and Q_{sum} refers to the sum of the primary side three-phase reactive power.

Based on Chinese national standards [19], it is possible to compensate the severe 3, 5 and 7th harmonic currents to their allowable values I_3*, I_5* and I_7*, and the other harmonics are fully compensated, so that the harmonic distortion rate can be met. In addition, the compensation capacity of a device can be reduced. Let $I_{\alpha Lh}$ and $I_{\beta Lh}$ be the effective values of the harmonic currents generated on the α and β power supply arms, respectively. For the 3rd, 5th and 7th harmonics, the optimized compensation currents are $I_{\alpha Lh}'$ and $I_{\beta Lh}'$. Then the harmonic energy required for harmonic optimization on the two arms are:

$$S_{c\alpha} = U_\alpha \left(\sqrt{\sum_{h=2}^{\infty} I_{\alpha Lh}^2} - \sqrt{\sum_{h=3、5、7} \left(I'_{\alpha Lh} \right)^2} \right) \tag{13}$$

$$S_{c\beta} = U_\beta \left(\sqrt{\sum_{h=2}^{\infty} I_{\beta Lh}^2} - \sqrt{\sum_{h=3、5、7} \left(I'_{\beta Lh} \right)^2} \right) \tag{14}$$

The total harmonic compensation power is $S_c = S_{c\alpha} + S_{c\beta}$.

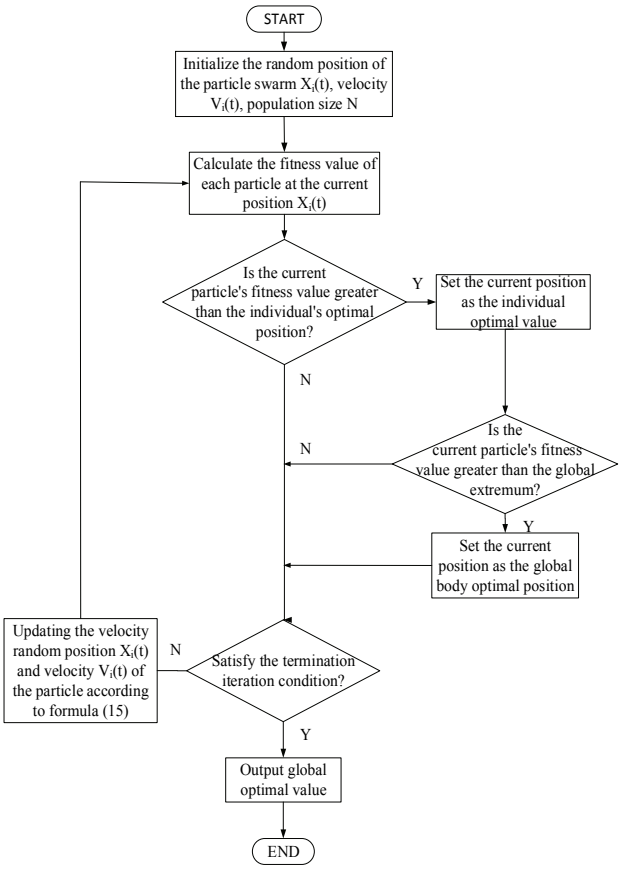

Fig. 3. Flow chart for solving the optimization model.

TABLE I
PARAMETERS OF PARTICLE SWARM OPTIMIZATION

Particle group N	20
Number of iterations	50
Maximum inertia weight value ω_{max}	0.9
Minimum inertia weight value ω_{max}	0.4
Learning factors c_1, c_2	0.5

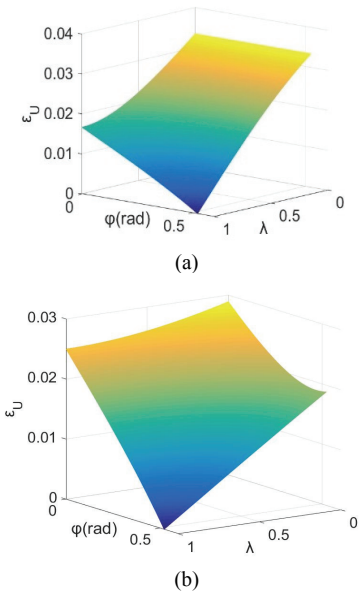

Fig. 4. Diagram of the relationship among ε_U, λ and φ under two working conditions. (a) Working condition 1. (b) Working condition 2.

III. ANALYSIS OF RPC CONTROL STRATEGY AND OPTIMAL COMPENSATION BASED ON PSO

A. Particle Swarm Optimization

As can be seen from the analysis in Section II, this is a complex constrained nonlinear optimization problem, which can be solved by reference to related algorithms. Currently, there are many algorithms for solving the above problems. The Particle Swarm Optimization (PSO) algorithm was developed by Kennedy and Eberhart [28], [29] in 1995. An optimization algorithm proposed to study the interaction between communities and environments is composed of simple individuals. Assume that in the D-dimensional search space, the population size of the particle group is N. The position is $x_i = [x_{i1}, x_{i2}, \ldots x_{iD}]$, and the flight speed is $v_i = [v_{i1}, v_{i2}, \ldots v_{iD}]$. In the t-th iteration, the particle's own historical optimal position is p_{best}, the global particle optimal position is g_{best}, and the particle is continuously updating its speed and position. The evolution equation of PSO can be described as:

$$\begin{cases} v_{ij}(t+1) = v_{ij}(t) + c_1 r_{1j}(t)\left(p_{best}(t) - x_{ij}(t)\right) \\ \quad +c_2 r_{2j}(t)(g_{best}(t) - x_{ij}(t)) \\ x_{ij}(t+1) = x_{ij}(t) + v_{ij}(t+1) \end{cases} \quad (15)$$

Where c_1, c_2 are learning factors, and r_1, r_2 are two independent random functions.

Particle swarm optimization is similar to a genetic algorithm, which is also an optimization algorithm. However, a particle swarm optimization algorithm does not have the evolutionary rules of mutation, crossover and selection of GA algorithms. The coding method is simpler than the latter, easier to implement, and there are not many parameters that need to be adjusted. The optimal solution can be found faster and more efficiently through an adjustment of each particle. In this paper, a particle swarm optimization algorithm is used to solve the problem. The parameters of the particle swarm algorithm are shown in Table I. The specific solution flow is shown in Fig. 3.

B. Case Analysis under Two Operating Conditions based on PSO

In order to analyze the relationships among variables, two different working conditions are designed for calculations assuming $I_{\alpha l} > I_{\beta l}$. These conditions are working condition 1: α arm active load 1000 W, β arm no load; and working condition 2: α arm active load 1000 W, β arm active load 500 W. According to formula (12), a relationship diagram among ε_U, λ and φ is obtained, as shown in Fig. 4.

TABLE II
COMPARISON OF PARAMETERS BEFORE AND AFTER OPTIMIZATION OF THE TWO WORKING CONDITIONS

		ε_U	λ	φ(rad)	S(VA)	Fall percentage (%)
working condition 1	Before optimization	0%	1	$\pi/6$	577.33	13.97%
	after optimization	1.4%	0.8624	0.3102	496.68	
working condition 2	Before optimization	0%	1	$\pi/6$	330.67	13.67%
	after optimization	1.3%	0.8056	0.4083	285.46	

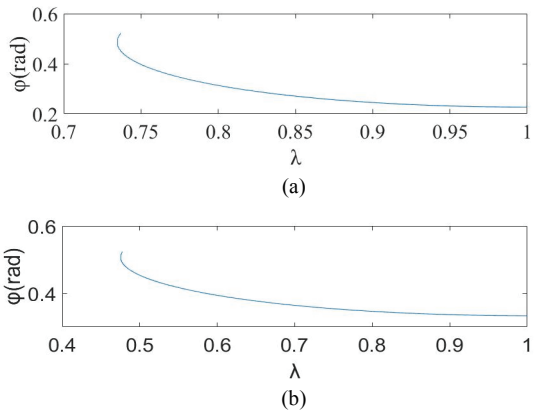

Fig. 5. Diagram of the relationship between λ and φ when ε_U = 2% under two working conditions. (a) Working condition 1. (b) Working condition 2.

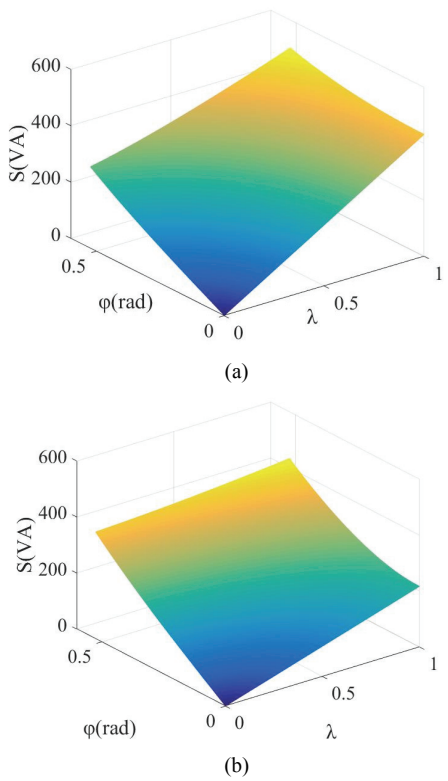

Fig. 6. Diagram of the relationships among S, λ and φ under two working conditions. (a) Working condition 1. (b) Working condition 2.

The relationship between λ and φ for the above two operating conditions is shown in Fig. 5.

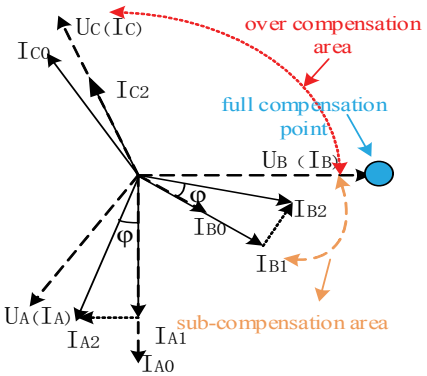

Fig. 7. Regional diagram of the output of the RPC.

Furthermore, a variable relationship diagram of the RPC compensation power S, λ and φ under various operating conditions can be obtained, as shown in Fig. 6.

When $\varepsilon_{U=}$ 2%, the intersection of the λ, φ curve and the S-λ-φ surface under each working condition is the power point of the RPC when the voltage unbalance is 2%, and the point that obtains the minimum value of S is the optimized point. In the minimum power point, at this time, the values of λ and φ are optimized values. The above two conditions are calculated to get Table II. By using this optimal method, the apparent power has nearly a 13% reduction. At the same time, ε_U meet the requirements.

C. RPC Output Principle and Control Strategy

Fig. 7 is a schematic diagram of the RPC output. According to the amount of reactive power compensation, it can be divided into sub-compensation, full compensation and over-compensation areas. Due to the symmetry of the α and β power supply arms, only one phase is listed.

The state of under-compensation is determined according to the requirements of the negative sequence imbalance ε_U, that is, the magnitude of ε_U determines the phase angle φ.

At this time, the primary current of the traction grid is changed from I_{A1}, I_{B1} to I_{A2}, I_{B2}. Once the phase angle reaches 60 degrees, the full compensation point is reached. At this time, the primary side currents I_A, I_B and I_C of the traction grid are in phase with the grid voltage, and the amplitudes are equal. If the reactive power compensation is continued, over-compensation occurs. Generally, this area does not want to appear. An RPC control strategy block diagram is shown in Fig. 8.

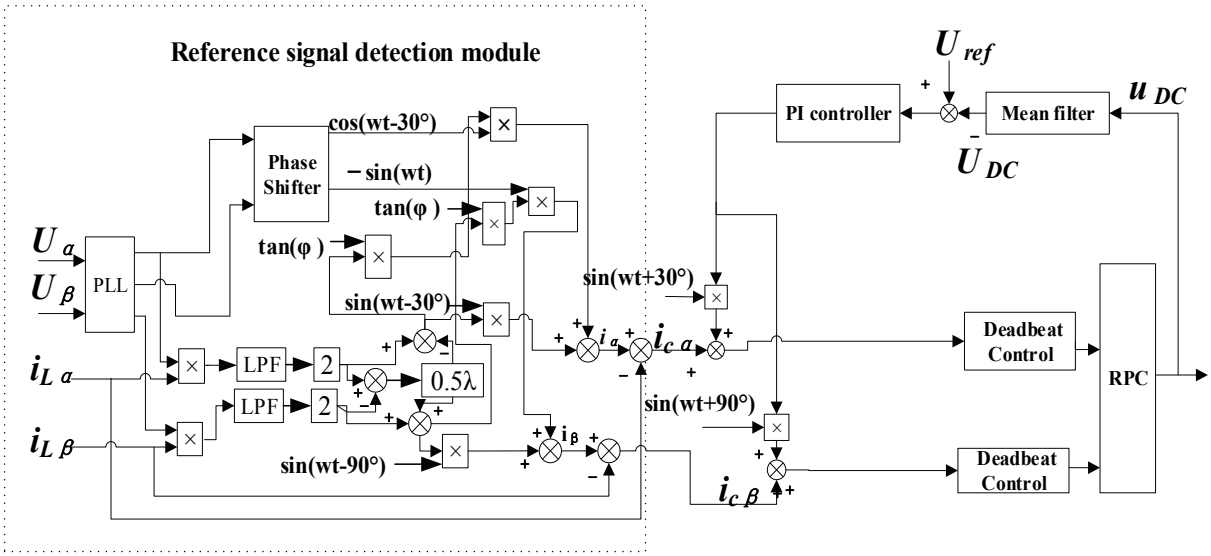

Fig. 8. Control block diagram of the RPC optimization compensation control strategy.

It can be seen from Fig. 8 that according to the relationship of the energy balance, the DC side voltage outer loop adopts a regulator based on precise feedback. In addition, the voltage error is processed by the regulator and multiplied by the synchronization signals of the two power supply arms to obtain two inverters of the RPC. The DC side voltage adjustment signal is superimposed with the current reference signal obtained by the detection link to obtain the actual current reference signals of the two converters. The traditional control method directly gives the actual current reference signal as the current inner loop, and the system can work normally under the rated load condition.

Using the predictive deadbeat control method, the transient characteristics of the RPC are faster, and the waveform control effect is guaranteed. Moreover, this predictive deadbeat method can improve the adaptability of the system to changes of the inductance parameters and it increases the robustness of the system.

IV. Simulation and Experimental Results

A. Simulation Results

In order to verify the above theory, a simulation model was built using MATLAB. The simulation parameters are as follows.

Three working conditions were designed for the simulation verification. The simulation model is built with reference to the RPC topology. The simulation time is set to 0.1 s, and the compensation device is input at 0.04 s. In working condition 1: the α side active power is 7 MW, while the reactive power is 3 Mvar, and the β side is under no-load. In working condition 2: the α side active power is 7 MW and the reactive power is 3 Mvar, while the β side active power is 3 MW and the reactive power is 2 Mvar. In working condition 3: the β side active power is 7 MW, while the reactive power is 3 Mvar, and the α side is under no-load, then at 0.1 s, the load of the α power supply arm abruptly rises to 4 MW. The dynamic compensation of the RPC can be observed.

TABLE III
RPC Simulation Parameters

Three-phase voltage	220 kV
V/v transformer ratio	220:27.5
Grid impedance resistance	0.2 Ω
Grid impedance inductance	0.1 mH
DC side capacitor	20 mF
Isolation transformer ratio	27.5：1.5

The simulation results for working condition 1 show that before the compensation, the α arm has a heavy current, and the β phase current is zero. On the three-phase bus side, the B phase is 0, and the C phase and A phase currents are opposite by the same value. After the RPC is input, the β arm shows a compensation current, and the phase changes. For working condition 2, after RPC compensation, the amplitude difference between the two-phase power supply arms of α and β is reduced, and the phase changes. For working condition 3, Fig. 9(c) shows the dynamic change of the waveform under the optimized compensation of the RPC device. The working condition 3 experiment is in real-time. It can be seen that the RPC has a good control effect, the capacity is optimized, and the economy is improved. Waveforms of this are shown in Fig. 9.

B. Experimental Results

In order to verify the feasibility of the active power, reactive power transfer and compensation algorithm of the RPC experimental platform, a V/v traction power supply system is built. Two single-phase transformers are used to form the equivalent structure of the V/v traction transformer, which connects the two power supply arms to a 220 V three-phase

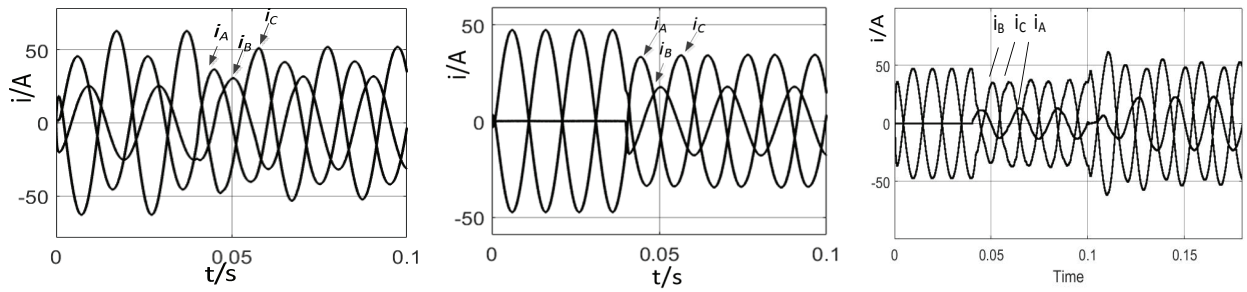

Fig. 9. Three bus current waveforms under three conditions. (a) Working condition 1. (b) Working condition 2. (c) Working condition 3.

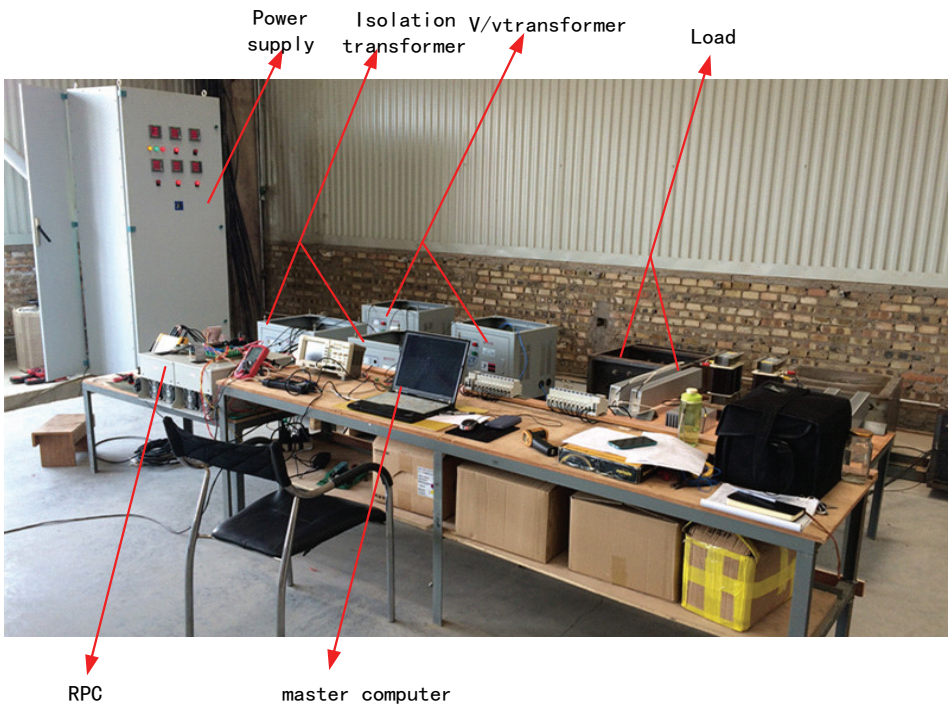

Fig. 10. Picture of the experimental platform.

TABLE IV
EXPERIMENTAL PARAMETERS

Parameters	Values	Parameters	Values
U_{AB}, U_{BC}, U_{CA}/V	380	N1:N2	1:1
U_{ac} , U_{bc}/V	220	L1,L2/mH	0.7
PF_{load}	0.85	C/uF	2000

bus-bar power supply network. The RPC main circuit board is connected to a power supply arm through a 1:1 isolation transformer, and the entire RPC main circuit is controlled by a TMS320F28335 DSP chip. The experimental switching frequency is k=5000 Hz. The experimental results are recorded by a FLUKE_435. Part of the experimental device is shown in Fig. 10. The RPC experimental device is shown in Fig. 11. The α phase is loaded, the load power factor is 0.85, and the β phase remains unloaded. The experimental parameters of the platform are shown in Table IV.

In the experiment, the DC side voltage is raised to 400V. In order to test the optimization capability of the proposed algorithm, two working conditions were designed for the experiment. Working condition 1 is where the load is only on one side. This situation is an extreme working situation. The transfer power is large when using the full compensation strategy. After using the particle swarm optimization algorithm, the current waveform and power quality data can be obtained as shown in Fig. 13. The current on the load side is slightly reduced, and the active current is turned from the load side to the no-load side. The α phase current is 57.9 A, the β phase current is 4.1 A, and the c phase current is 53.6 A. The voltage unbalance is 3.8%, which exceeds the specified requirements which reduce it to 1.2% after optimization compensation. At this time, because the full compensation strategy is not adopted, the phase difference among the 3 phase currents is not 120°. Working condition 2 is where the load is on both sides.

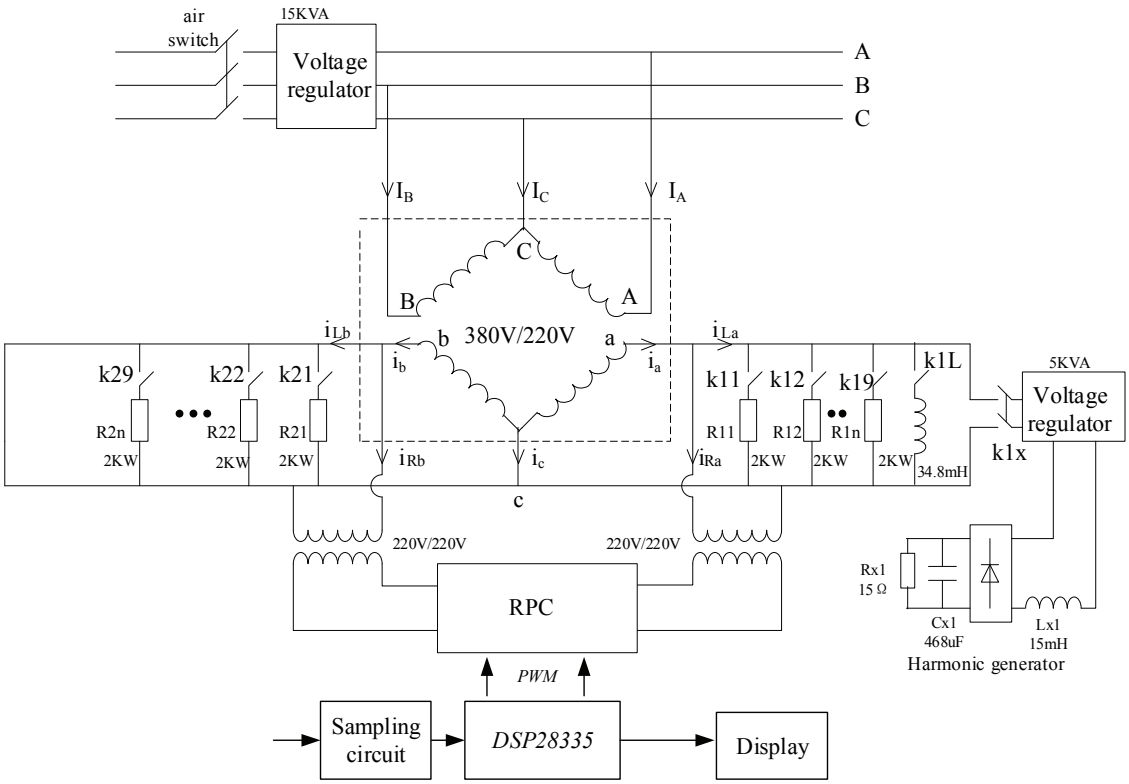

Fig. 11. RPC experiment device.

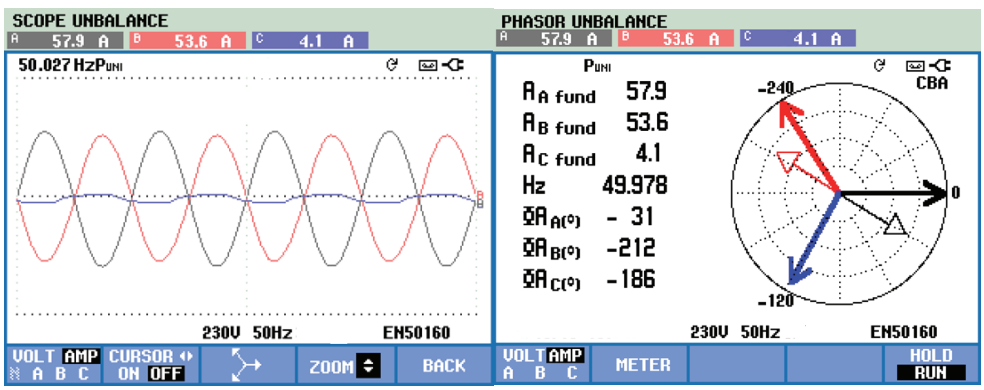

Fig. 12. Current waveform and power quality data before the compensation of working condition 1.

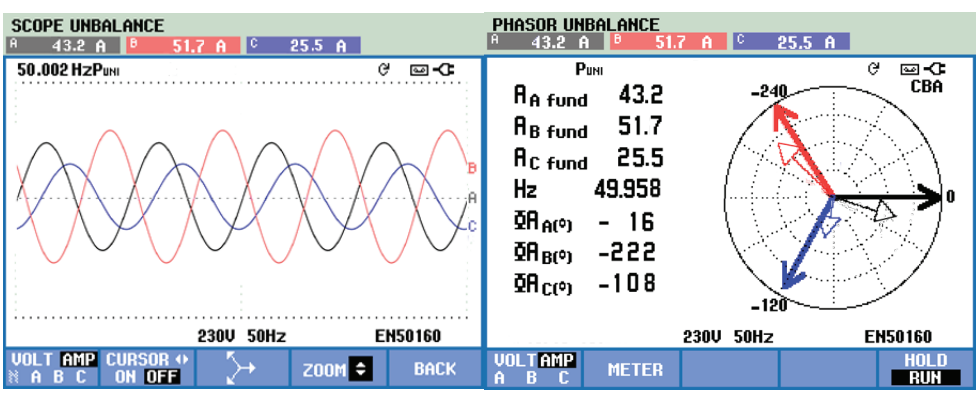

Fig. 13. Current waveform and power quality data for the optimal compensation of working condition 1.

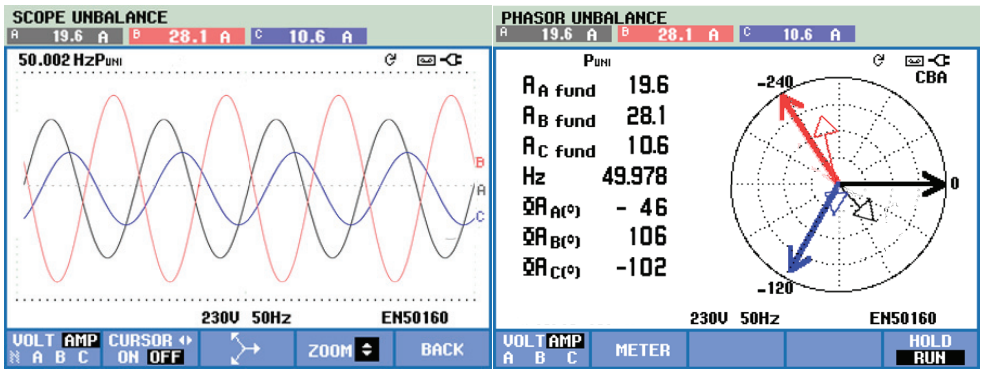

Fig. 14. Current waveform and power quality data before the compensation of working condition 2.

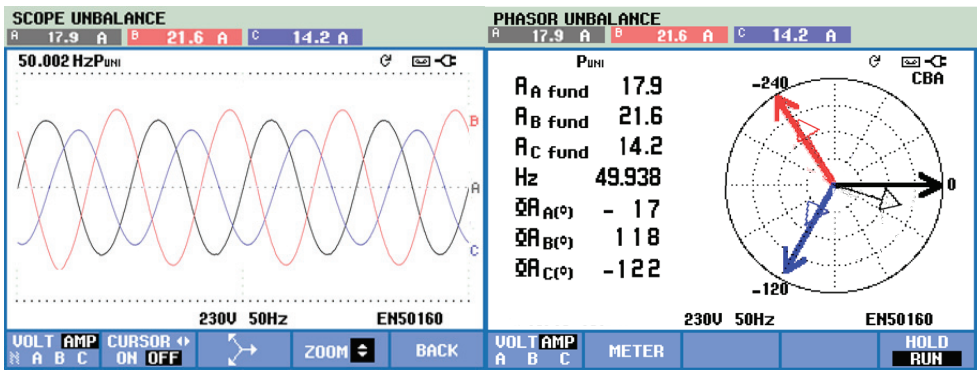

Fig. 15. Current waveform and power quality data of the optimal compensation of working condition 2.

TABLE V
COMPARISON OF VOLTAGE IMBALANCE BEFORE AND AFTER COMPENSATION

	Voltage imbalance before compensation ε_U/%	Voltage imbalance after compensation ε_U/%
Working condition 1	3.8	1.2
Working condition 2	2.8	1.1

It can be seen from the Fig. 14 that the current of the α power supply arm is 19.6A, and the current of the β power supply arm is 10.6A. After the optimized compensation, the currents of the two power supply arms are 17.9A and 14.2A. The transferred active current is less, and the RPC compensation energy is reduced. The voltage unbalance is 2.8% before compensation and it is reduced to 1.1% after optimal compensation. Compare the changes in voltage imbalance before and after compensation. The specifics are shown in Table V. The three-phase bus current waveform and power quality data after compensation are shown in Fig. 15.

The above example shows that the PSO algorithm is well adapted for RPC capacity optimization compensation. The optimal solution for the compensation coefficient in the global range under the premise of achieving basic power quality can be obtained. The minimum compensation capacity is required. After optimization compensation, the power factor of operating condition 1 can be stabilized at 0.96 and working condition 2 can reach 0.98.

V. CONCLUSION

In this paper, the principle of complete compensation and optimal compensation of the RPC are analyzed. According to a comparison of vector diagrams, the feasibility of the optimal compensation strategy is theoretically verified. The compensation effect is related to the compensation coefficient λ, the power factor PF, and the negative sequence imbalance ε_U. In addition, the optimal solution is obtained by using the relevant constraint conditions. A particle swarm optimization algorithm is used to solve the problem. The compensation coefficient can be obtained in the global range. Adopting this optimization strategy can reduce the compensation capacity of the RPC device. It can also meet power quality requirements and improve the economics of the device. According to obtained results, the proposed compensation strategy has a good character. This algorithm has practical significance in electrified railways.

REFERENCES

[1] H. M. Roudsari, A. Jalilian, and S. Jamali, "Resonance assessment in electrified railway systems using comprehensive model of train and overhead catenary system," in *IEEE Int.*

Conf. Ind. Tech, pp. 1142-1148, Mar. 2015,

[2] D. Zhang, Z. Zhang, W. Wang, and Y. Yang, "Negative sequence current optimizing control based on railway static power conditioner in V/v traction power supply system," *IEEE Trans. Power Electron.*, Vol. 31, No. 1, pp. 200-212, Jan. 2016.

[3] L. Fang, A. Luo, X. Xu, and H. Fang, "A novel power quality compensator for negative-sequence and harmonic currents in high-speed electric railway," in *Proc. Asia-Pacific Power Energy Eng. Conf*, pp. 1-5, Mar. 2011.

[4] B. Chen, C. Zhang, W. Zeng, C. Tian, and J. Yuan, "An electrical-magnetic hybrid power quality compensation strategy for V/V traction power supply system," in Proc. *Energy Convers. Congr. Expo*, pp. 3774-3779, Sep. 2014.

[5] S. Hu, B. Xie, Y. Li, X. Gao, Z. Zhang, L. Luo, Krause. Olav, and Yijia. Cao, "A power factor oriented railway power flow controller for power quality improvement in electrical railway power system," *IEEE Trans. Ind. Electron*., Vol. 64, No. 2, pp. 1167-1177, Feb. 2017.

[6] T. Uzuka, "Faster than a speeding bullet: An overview of Japanese high-speed rail technology and electrification," *IEEE Electrific. Mag.*, Vol. 1, No. 1, pp. 11-20, Sep. 2013.

[7] S. M. M. Gazafrudi, A. T. Langerudy, E. F. Fuchs, and K. AI-Haddad, "Power quality issues in railway electrification: A comprehensive perspective," *IEEE Trans. Ind. Electron*., Vol. 62, No. 5, pp. 3081-3090, May. 2015.

[8] S. T. Senini and P. Wolfs, "Novel topology for correction of unbalanced load in single phase electric traction systems," in *Power Electron. Spec. Conf. (PESC)*, Vol. 3, pp. 1208-1212, 2002.

[9] W. Yingdong, J. Qirong, and Z. Xiujuan, "A novel control strategy for optimization of power capacity based on railway power static conditioner," in *23rd IEEE-Applied Power Electron. Conf. Expos.*, pp. 1669-1674, Feb. 2008.

[10] W. Chuanping, L. An, J. Shen, M. Fu Jun, and P. Shuangjian, "A negative sequence compensation method based on a two-phase three-wire converter for a high-speed railway traction power supply system," *IEEE Trans. Power Electron.,* Vol. 27, pp. 706-717, Feb. 2012.

[11] M. Fujun, L. An, X. Xianyong, X. Huagen, C. Wu, and W. Wang, "A simplified power conditioner based on half-bridge converter for high-speed railway," *IEEE Trans. Ind. Electron.,* Vol. 60, No. 2, pp. 728-738, Feb. 2013.

[12] F. Wang, J. Duarte, and M. Hendrix, "Pliant active and reactive power control for grid-interactive converters under unbalanced voltage dips," *IEEE Trans. Power Electron.*, Vol. 26, No. 5, pp. 1511-1521, May. 2011.

[13] S. L. Chen, F. C. Kao, and T. M. Lee, "Specification of minimum short circuit capacity for three-phase unbalance evaluation of high-speed railway power system," in *Proc. Int. Conf. Energ. Manag. Power Del.*, Vol. 1, pp. 323-330, Nov. 1995.

[14] B. Chen, C. Zhang, C. Tian, J. Wang, and J. Yuan, "A hybrid electrical magnetic power quality compensation system with minimum active compensation capacity for V/V cophase railway power supply system," *IEEE Trans. Power Electron.*, Vol. 31, No. 6, pp. 4159-4170, Jun. 2016.

[15] L. Wu and M. Wu, "Single-phase Cascaded H-bridge Multilevel active Power Filters in AC Electric Railway Systems." *J. Power Electron.*, Vol. 17, No 3, pp. 788-797, May 2017.

[16] Z. He, H. Hu, Y. Zhang, and S. Gao, "Harmonic resonance assessment to traction power-supply system considering train model in China high-speed railway," *IEEE Trans. Power Del.*, Vol. 29, No. 7, pp. 1735-1743, Aug. 2014.

[17] H. Hu, Z. He, X. Li, K. Wang, and S. Gao, "Power quality impact assessment for high-speed railway associated with high-speed trains using traintimetable – Part I: Methodology and modeling," *IEEE Trans. Power Del.*, Vol. 31, No. 2, pp. 693-703, Apr. 2016.

[18] *IEEE Recommended Practice for Monitoring Electric Power Quality*, IEEE Std 1159-1995, 1995.

[19] *Quality of Electric Energy Harmonics in public supply netwoek*, National Standard GB/T 14549-1993, 1993

[20] H. Wang, Y. Liu, K. Yan, Y. Fu, and C. Zhang, "Analysis of static var compensators installed in different positions in electric railways," *IET Elect. Syst. Transp*., Vol. 5, No. 3, pp. 129-134, Sep. 2015.

[21] N. Y. Dai, M. C. Wong, K. W. Lao, and C. K. Wong, "Modelling and control of a railway power conditioner in co-phase traction power system under partial compensation," *IET Power Electron*., Vol. 7, No. 5, pp. 1044-1054, May 2014.

[22] S. Hu, Z. W. Zhang, Y. H. Chen, G. D. Zhou, Y. Li, L. F. Luo, Y. J. Cao, B. Xie, X. T. Chen, and B. Wu, "A new integrated hybrid power quality control system for electrical railway," *IEEE Trans. Ind. Electron*., Vol. 62, No. 10,pp. 6222-6232, Oct. 2015.

[23] Z. Zhang, B. Wu, J. Kang, and L. Luo, "A multi-purpose balanced transformer for railway traction applications," *IEEE Trans. Power Del.*, Vol. 24, No. 2, pp. 711-718, Apr. 2009

[24] A. Luo, F. Ma, C. Wu, S. Q. Ding, Q.-C. Zhong, and Z. K. Shuai," A dual-loop control strategy of railway static power regulator under V/V electric traction system," *IEEE Trans. Power Electron.*, Vol. 26, No. 7, pp. 2079-2091, Jul. 2011.

[25] S. Babaei, B. Fardanesh, and S. Bhattacharya, "High-power VSC-based simultaneous positive- and negative-sequence voltage regulator," *IEEE Trans. Power Del.*, Vol. 29, No. 5, pp. 2124-2135, Oct. 2014.

[26] S. Hu, Z. Zhang, Y. Li, L. Luo, Y. Cao, and C. Rehtanz, "A new half-bridge winding compensation-based power conditioning system for electric railway with LQRI," *IEEE Trans. Power Electron.*, Vol. 29, No. 10, pp. 5242-5256, Oct. 2014.

[27] Z. Shuai, A. Luo, J. Shen, and X. Wang, "Double closed-loop control method for injection-type hybrid active power filter," *IEEE Trans. Power Electron.*, Vol. 26, No. 9, pp. 2393-2403, Sep. 2011.

[28] R. Eberhart and J. Kennedy, "A new optimizer using particle swarm theory," *Proc. 6 Int. Symposium on Micro Machine and Human Science*, pp. 39-43, 1995.

[29] J. Kennedy and R. Eberhart, "Particle Swarm Optimization," *IEEE International Conference on Neural Networks (Perth, Australia)*, pp. 1942-1948, 1995.

Youhua Jiang was born in Nancheng, China. He obtained his M.S. and Ph.D. degrees from Shanghai University, Shanghai, China, in 2000 and 2006, respectively. He engaged in postdoctoral work at Hangzhou Qianjiang Electric Company, Hangzhou, China, from 2006 to 2008. He has been employed at the Shanghai University of Electric Power, Shanghai, China, since 2008, where he is presently working as a Professor and Master Tutor in the College of Electronics and Information Engineering. His current research interests include power quality, harmonic control, reactive power optimization and power electronics.

Wenji Wang was born in Wuhan, China, in 1993. He obtained his B.S. degree in Electrical Engineering and Automation from Three Gorges University, Yichang, China, in 2016; and his M.S. degree from the Shanghai University of Electric Power, Shanghai, China, in 2019. He is presently working for the State Grid Wuhan Electric Power Company, Wuhan, China. His current research interests include power electronics and power quality optimization.

Xiangwei Jiang was born in Anqing, China, in 1991. He obtained his Ph.D. degree from the Shanghai University of Electric Power, Shanghai, China, in 2018. He is presently working for the State Grid Anqing Electric Power Company, Anqing, China. His current research interests include power electronics technology and reactive power quality.

Le Zhao was born in Songzi, China. He obtained his M.S. degree from the Shanghai University of Electric Power, Shanghai, China, in 2017. He is presently working for the Shanghai Electric Power Research Institute, Shanghai, China. His current research interests include power system and power electronics technology.

Yilong Cao was born in Dangtu, China, in 1965. He obtained his B.S. degree from the Department of Electrical Engineering, Anhui University of Science and Technology, Anhui, China, in 1985; and his M.S. degree from the Department of Marine Electrical Engineering, Naval University of Engineering, Wuhan, China, in 1988. He has been employed at the Shanghai University of Electric Power, Shanghai, China, since 2005, where he is presently working as a Professor and Master Tutor in the College of Electronics and Information Engineering. His current research interests include power electronics, electric drives, electronic information and electrical automation.